PROCEEDINGS A

rspa.royalsocietypublishing.org

Research

Cite this article: Gao L, Audouze C, Nair PB. 2015 Anchored analysis of variance Petrov–Galerkin projection schemes for linear stochastic structural dynamics. *Proc. R. Soc. A* **471**: 20150023.
http://dx.doi.org/10.1098/rspa.2015.0023

Received: 11 February 2015
Accepted: 21 September 2015

Subject Areas:
structural engineering, computational mathematics, mathematical modelling

Keywords:
stochastic structural dynamics, curse of dimensionality, functional ANOVA decomposition, Petrov–Galerkin, polynomial chaos expansions, stochastic ordinary differential equations

Author for correspondence:
Prasanth B. Nair
e-mail: pbn@utias.utoronto.ca

Electronic supplementary material is available at http://dx.doi.org/10.1098/rspa.2015.0023 or via http://rspa.royalsocietypublishing.org.

THE ROYAL SOCIETY PUBLISHING

Anchored analysis of variance Petrov–Galerkin projection schemes for linear stochastic structural dynamics

Lin Gao, Christophe Audouze and Prasanth B. Nair

University of Toronto Institute for Aerospace Studies, 4925 Dufferin Street, Toronto, Ontario, Canada M3H 5T6

In this paper, we propose anchored functional analysis of variance Petrov–Galerkin (AAPG) projection schemes, originally developed in the context of parabolic stochastic partial differential equations (Audouze C, Nair PB. 2014 *Comput. Methods Appl. Mech. Eng.* **276**, 362–395. (doi:10.1016/j.cma.2014.02.023)) for solving a class of problems in linear stochastic structural dynamics. We consider the semi-discrete form of the governing equations in the time-domain and the proposed formulation involves approximating the dynamic response using a Hoeffding functional analysis of variance decomposition. Subsequently, we design a set of test functions for a stochastic Petrov–Galerkin projection scheme that enables the original high-dimensional problem to be decomposed into a sequence of decoupled low-dimensional subproblems that can be solved independently of each other. Numerical results are presented to demonstrate the efficiency and accuracy of AAPG projection schemes and comparisons are made to approximations obtained using Monte Carlo simulation, generalized polynomial chaos-based stochastic Galerkin projection schemes and the generalized spectral decomposition method. The results obtained suggest that the proposed approach holds significant potential for alleviating the curse of dimensionality encountered in tackling high-dimensional problems in stochastic structural dynamics with a large number of spatial and stochastic degrees of freedom.

1. Introduction

In this paper, we are concerned with efficient numerical methods for solving systems of second-order stochastic

ordinary differential equations (SODEs) arising in linear stochastic structural dynamics of the form

$$\mathbf{M}(\boldsymbol{\xi})\ddot{\mathbf{u}}(\boldsymbol{\xi},t)+\mathbf{K}(\boldsymbol{\xi})\mathbf{u}(\boldsymbol{\xi},t)+\mathbf{C}(\boldsymbol{\xi})\dot{\mathbf{u}}(\boldsymbol{\xi},t)=\mathbf{f}(\boldsymbol{\xi},t)\ \text{a.s.}\quad \text{in } \Gamma\times[0,T], \tag{1.1}$$

where $\mathbf{M}(\boldsymbol{\xi})\in\mathbb{R}^{n\times n}$, $\mathbf{K}(\boldsymbol{\xi})\in\mathbb{R}^{n\times n}$ and $\mathbf{C}(\boldsymbol{\xi})\in\mathbb{R}^{n\times n}$ denote the stochastic mass, stiffness and damping matrices, respectively, $\mathbf{u}\in\mathbb{R}^n$ is the displacement vector, $t\in[0,T]$ denotes time ($T<+\infty$) and n is the total number of degrees of freedom (d.f.). The external force $\mathbf{f}(\boldsymbol{\xi},t)\in\mathbb{R}^n$ is assumed to be a time-dependent stochastic process. We denote the probability space by the triplet $(\Omega,\mathcal{F},\mathcal{P})$, where $\Omega\subset\mathbb{R}^q$ is the sample space, $\mathcal{F}$ is the σ-algebra associated with Ω and $\mathcal{P}:\mathcal{F}\to[0,1]$ is a probability measure. The components of the vector $\boldsymbol{\xi}=(\xi_1,\xi_2,\ldots,\xi_N)^{\mathrm{T}}:\Omega\to\mathbb{R}^N$ are assumed to be a set of independent random variables whose joint probability density function (PDF) can be written as the product of its marginal densities, i.e. $\rho(\boldsymbol{\xi})=\prod_{i=1}^{N}\rho_i(\xi_i)$. We denote by $\Gamma=\Gamma_1\times\cdots\times\Gamma_N$ the joint image of $\boldsymbol{\xi}$. The governing SODEs (1.1) are supplemented with the following stochastic initial conditions

$$\mathbf{u}(\boldsymbol{\xi},0)=\mathbf{Z}_0(\boldsymbol{\xi}),\quad \dot{\mathbf{u}}(\boldsymbol{\xi},0)=\mathbf{Z}_1(\boldsymbol{\xi}),\quad \text{where } \mathbf{Z}_0(\boldsymbol{\xi}),\mathbf{Z}_1(\boldsymbol{\xi})\in\mathbb{R}^n. \tag{1.2}$$

The equations considered here are essentially the semi-discrete form of the governing equations in the time-domain obtained by spatial and random field discretization of stochastic partial differential equations (SPDEs) encountered in linear elastodynamics. The model structure considered is fairly general and allows for the consideration of uncertainties arising from constitutive model parameters, geometry, initial conditions, boundary conditions, forcing functions, etc. It is worth noting that the solution of (1.1) is parametrized in terms of the same set of random variables used in the parametrization of the matrices and the source term. Indeed, from an SPDE point of view, it follows from the Doob–Dynkin's lemma [1] that when the SPDE coefficients and/or the source term depend on $\boldsymbol{\xi}\in\mathbb{R}^N$, then the SPDE solution can be described using the same set of random variables.

A commonly used approach to solve (1.1) is the Monte Carlo simulation (MCS) technique and its variants [2,3]. Even though simulation methods are versatile and general purpose in scope, their convergence rate is low and they can become computationally very expensive for systems with a large number of degree of freedom (d.f). This has motivated research into alternative approximation methods that can provide computational cost savings (see, for example, [4–9] and the references therein). There is also a wide body of literature in dynamics of uncertain structural systems that focuses on non-parametric uncertainty models [10–14] and situations where a non-probabilistic model of uncertainty is more appropriate [15,16]. The focus of this paper is on parametric uncertainty models wherein the joint PDF of the random vector $\boldsymbol{\xi}$ is specified and it is sought to approximate the statistics of the dynamic response, $\mathbf{u}(\boldsymbol{\xi},t)$, as a function of time.

In 1991, Ghanem & Spanos [17] proposed the application of polynomial chaos (PC) expansions in conjunction with Galerkin projection to solve a range of stochastic operator equations. In the context of equation (1.1), this approach involves approximating the solution using a PC expansion as follows

$$\mathbf{u}(\boldsymbol{\xi},t)\approx\hat{\mathbf{u}}(\boldsymbol{\xi},t)=\sum_{i=0}^{P}\mathbf{u}_i(t)\varphi_i(\boldsymbol{\xi}), \tag{1.3}$$

where $\mathbf{u}_i(t)\in\mathbb{R}^n$ are undetermined vector functions of time and $\varphi_i(\boldsymbol{\xi})$, $i=0,1,2,\ldots,P$ denotes a set of orthonormal PC basis functions, i.e. $\varphi_0=1$, $\langle\varphi_i\varphi_j\rangle=\delta_{ij}$, where $\langle\cdot\rangle=\int_\Gamma\cdot\,\rho(\boldsymbol{\xi})\,\mathrm{d}\boldsymbol{\xi}$ and δ_{ij} denotes the Kronecker delta [17]. In the original work of Ghanem & Spanos [17], Hermite polynomials were used as basis functions in conjunction with Galerkin projection. As shown later by Xiu & Karniadakis [18], orthogonal polynomials from the Askey family can be used to construct a generalized PC (gPC) expansion. The number of terms in the expansion is given by $P+1=(N+p)!/(N!p!)$, where N is the number of random variables and p is the gPC expansion

order. The undetermined coefficients in (1.3) can be calculated by applying the stochastic Galerkin projection scheme, which involves the enforcement of the following orthogonality conditions

$$\mathbf{M}(\boldsymbol{\xi})\ddot{\hat{\mathbf{u}}}(\boldsymbol{\xi},t)+\mathbf{K}(\boldsymbol{\xi})\hat{\mathbf{u}}(\boldsymbol{\xi},t)+\mathbf{C}(\boldsymbol{\xi})\dot{\hat{\mathbf{u}}}(\boldsymbol{\xi},t)-\mathbf{f}(\boldsymbol{\xi},t)\perp\varphi_i(\boldsymbol{\xi}),\quad i=0,1,2,\ldots,P \tag{1.4}$$

and

$$\hat{\mathbf{u}}(\boldsymbol{\xi},0)-\mathbf{Z}_0(\boldsymbol{\xi})\perp\varphi_i(\boldsymbol{\xi})\quad\text{and}\quad\dot{\hat{\mathbf{u}}}(\boldsymbol{\xi},0)-\mathbf{Z}_1(\boldsymbol{\xi})\perp\varphi_i(\boldsymbol{\xi}),\quad i=0,1,2,\ldots,P. \tag{1.5}$$

The preceding orthogonality conditions lead to a coupled system of $n(P+1)$ deterministic ODEs that can be integrated using a standard time marching scheme to estimate the undetermined coefficients in (1.3). This approach has been shown to provide good approximations with computational effort significantly lower than simulation methods for a large class of problems [19–22]. However, the computational cost associated with solving the equations arising from stochastic Galerkin projection can become prohibitive when employing high-order gPC expansions for large-scale systems even with a modest number of random variables. This has motivated research into alternative decomposition strategies that can be more efficient than gPC-based stochastic Galerkin methods; see, for example, sparse gPC expansions [23], the generalized spectral decomposition (GSD) technique and its variants [24–27], and dynamically orthogonal field equation methods [28,29]. These approaches are yet to be applied in the context of stochastic structural dynamics, the only exception being the work of Chevreuil & Nouy [30], which proposes a proper generalized decomposition scheme for frequency domain analysis of structural systems.

Another function decomposition scheme that has been widely studied in various fields is the Hoeffding functional analysis of variance (ANOVA) representation [31–34]. This approach has been successfully applied within both non-intrusive [35–38] and intrusive settings [39,40] to solve uncertainty quantification problems. More recently, Audouze & Nair [40] proposed the anchored ANOVA Petrov–Galerkin (AAPG) projection scheme for solving high-dimensional parabolic SPDEs. In this work, it was shown that by using an anchored ANOVA decomposition in conjunction with an appropriate test space, the original high-dimensional weak form can be decoupled into low-dimensional subproblems that can be solved independently of each other. As a result, the AAPG projection scheme holds significant potential for alleviating the curse of dimensionality that is inevitable when applying gPC-based stochastic Galerkin projection schemes to stochastic operator equations. Theoretical analysis and numerical studies conducted so far suggest that AAPG schemes provide accuracy comparable to the gPC-based stochastic Galerkin projection scheme while offering significant computational cost savings for high-dimensional SPDE models.

The focus of this paper is to formulate an AAPG projection scheme to efficiently solve high-dimensional SODEs encountered in linear stochastic structural dynamics. We shall show that by considering the weighted residual form of (1.1) along with an anchored functional ANOVA decomposition of the solution and suitable test functions, it becomes possible to decouple the original high-dimensional equation into a set of *decoupled* low-dimensional subproblems. Numerical studies will be presented for a set of problems to illustrate the efficacy of the proposed approach and comparisons will be made against the classical gPC-based stochastic Galerkin projection scheme and a GSD scheme.

The remainder of this paper is organized as follows: §2 outlines the anchored ANOVA decomposition scheme and some of its theoretical properties. Section 3 provides the derivation of the AAPG projection scheme [40] in the special context of linear stochastic structural dynamical systems. This is followed by §4 where we present numerical results obtained using MCS, gPC, GSD and AAPG schemes for two case studies providing accuracy and performance comparisons. Section 5 concludes the paper and outlines some directions for future work.

2. Anchored ANOVA decomposition

We begin with approximating the solution of (1.1) using a Hoeffding functional ANOVA decomposition [31–34] of the form

$$\mathbf{u}(\boldsymbol{\xi},t) \approx \mathbf{u}^0(t) + \sum_{j_1=1}^{N} \mathbf{u}^{j_1}(\xi_{j_1},t) + \sum_{j_1<j_2}^{N} \mathbf{u}^{j_1 j_2}(\xi_{j_1},\xi_{j_2},t) + \sum_{j_1<j_2<j_3}^{N} \mathbf{u}^{j_1 j_2 j_3}(\xi_{j_1},\xi_{j_2},\xi_{j_3},t) + \cdots, \quad \boldsymbol{\xi} \in \Gamma \subset \mathbb{R}^N. \tag{2.1}$$

The first term $\mathbf{u}^0(t)$ in the decomposition is the zero-order component function which is a deterministic function of time. The first-order component function $\mathbf{u}^{j_1}$ is the independent contribution to $\mathbf{u}(\boldsymbol{\xi},t)$ by the random variable ξ_{j_1} acting alone. The second-order component function $\mathbf{u}^{j_1 j_2}$ denotes the pair correlated contribution to the solution by ξ_{j_1} and ξ_{j_2}. Similarly, the higher-order terms in (2.1) denote higher-order contributions by subsets of random variables. Note that all the component functions in the decomposition are functions of time.

The Lth-order functional ANOVA decomposition can be compactly rewritten as follows:

$$\mathbf{u}(\boldsymbol{\xi},t) \approx \mathbf{u}^L(\boldsymbol{\xi},t) = \mathbf{u}^0(t) + \sum_{k=1}^{L} \sum_{j_1<j_2<\cdots<j_k}^{N} \mathbf{u}^{j_1 j_2 \cdots j_k}(\xi_{j_1},\xi_{j_2},\ldots,\xi_{j_k},t), \quad 1 \le L \le N. \tag{2.2}$$

The main advantage of using a functional ANOVA decomposition arises from the fact that in various practical applications, higher-order interactions between random variables can be neglected, meaning that a small truncation order can be used in (2.2). In a wide range of high-dimensional problems, this feature can be exploited to design highly efficient numerical schemes [34]. Several examples are examined in reference [34] showing that in practice the truncation order L is generally small in applications such as molecular dynamics simulations or statistics (typically $2 \le L \le 4$). However, for data mining applications, the higher-order interactions may need to be considered ($L \ge 7$) [41]. We shall later show via numerical studies that a second-order functional ANOVA decomposition ($L = 2$) can provide good accuracy for a set of case studies in stochastic structural dynamics.

To ensure the uniqueness of the ANOVA decomposition, the following orthogonality constraints are imposed on the component functions

$$\left\langle \mathbf{u}^{j_1 \cdots j_s}(\xi_{j_1},\ldots,\xi_{j_s},t), \mathbf{u}^{k_1 \cdots k_p}(\xi_{k_1},\ldots,\xi_{k_p},t) \right\rangle_{\mu} = 0, \quad \text{for } (j_1,\ldots,j_s) \ne (k_1,\ldots,k_p). \tag{2.3}$$

Here, $\langle \cdot,\cdot \rangle_\mu$ denotes the L^2 inner product with respect to a certain measure $\mathrm{d}\mu(\boldsymbol{\xi})$, i.e. $\langle \mathbf{w}_1, \mathbf{w}_2 \rangle_\mu = \int_\Gamma \mathbf{w}_1^{\mathrm{T}}(\boldsymbol{\xi}) \mathbf{w}_2(\boldsymbol{\xi})\, \mathrm{d}\mu(\boldsymbol{\xi})$. The preceding orthogonality constraints are equivalent to imposing null integral constraints of the form

$$\int_{\Gamma_k} \mathbf{u}^{j_1 \cdots j_p}(\xi_{j_1},\ldots,\xi_{j_p},t)\, \mathrm{d}\mu_k(\xi_k) = 0, \quad \forall\, k \in \{j_1,\ldots,j_p\}. \tag{2.4}$$

In an anchored functional ANOVA decomposition, $\mathrm{d}\mu(\boldsymbol{\xi})$ is taken to be a Dirac product measure of the form [33,34]

$$\mathrm{d}\mu(\boldsymbol{\xi}) = \prod_{j=1}^{N} \mathrm{d}\mu_j(\xi_j) = \prod_{j=1}^{N} \delta\left(\xi_j - \xi_j^a\right) \mathrm{d}\xi_j, \tag{2.5}$$

where $\delta(\cdot)$ denotes the Dirac delta and $\boldsymbol{\xi}^{\mathrm{a}} = (\xi_1^{\mathrm{a}}, \xi_2^{\mathrm{a}}, \ldots, \xi_N^{\mathrm{a}})^{\mathrm{T}} \in \Gamma$ is the so-called *anchor point*. It was shown in references [33,42] that when using the Dirac product measure (2.5), the ANOVA

component functions in (2.2) can be written in terms of point evaluations as follows

$$\left.\begin{aligned} \mathbf{u}^0(t) &= \mathbf{u}(\boldsymbol{\xi}^{\mathrm{a}}, t), \\ \mathbf{u}^{j_1}(\xi_{j_1}, t) &= \mathbf{u}(\boldsymbol{\xi}^{\mathrm{a}}_{j_1}, t) - \mathbf{u}^0(t) \\ \text{and} \qquad \mathbf{u}^{j_1 j_2}(\xi_{j_1}, \xi_{j_2}, t) &= \mathbf{u}(\boldsymbol{\xi}^{\mathrm{a}}_{j_1 j_2}, t) - \mathbf{u}^{j_1}(\xi_{j_1}, t) - \mathbf{u}^{j_2}(\xi_{j_2}, t) - \mathbf{u}^0(t), \end{aligned}\right\} \tag{2.6}$$

or more generally,

$$\begin{aligned} \mathbf{u}^{j_1\cdots j_k}(\xi_{j_1}, \ldots, \xi_{j_k}, t) = \mathbf{u}(\boldsymbol{\xi}^{\mathrm{a}}_{j_1\cdots j_k}, t) &- \sum_{i_1<\cdots<i_{k-1}, i_l \in I_k} \mathbf{u}^{i_1\cdots i_{k-1}}(\xi_{i_1}, \ldots, \xi_{i_{k-1}}, t) \\ &- \sum_{i_1<\cdots<i_{k-2}, i_l \in I_k} \mathbf{u}^{i_1\cdots i_{k-2}}(\xi_{i_1}, \ldots, \xi_{i_{k-2}}, t) - \cdots\cdots - \sum_{i_1 \in I_k} \mathbf{u}^{i_1}(\xi_{i_1}, t) - \mathbf{u}^0(t), \end{aligned} \tag{2.7}$$

with $I_k = \{j_1, j_2, \ldots, j_k\}$. We denote by $\mathbf{u}(\boldsymbol{\xi}^{\mathrm{a}}_{j_1\cdots j_k}, t)$ the evaluation of $\mathbf{u}$ at the point $\boldsymbol{\xi}^{\mathrm{a}}_{j_1\cdots j_k}$, where $\xi_i, i \in I_k$ are active random variables and $\xi_i = \xi_i^a$ for $i \notin I_k$. In addition, the null integral constraints (2.4) using the Dirac product measure (2.5) become

$$\mathbf{u}^{j_1\cdots j_k}|_{\xi_i = \xi_i^a} = 0, \quad \forall\, i \in I_k. \tag{2.8}$$

The above property will be used later in the proof of theorem 3.1.

We shall next devise a stochastic Petrov–Galerkin projection scheme to set up equations that govern the evolution in time of the component functions in (2.2).

3. Anchored ANOVA Petrov–Galerkin projection scheme

Here, we introduce the stochastic-weighted residual form of (1.1) and show that by defining an appropriate test space, the original high-dimensional problem can be decoupled into stochastic low-dimensional subproblems that can be solved independently of each other. This is an important property of AAPG projection schemes that enables the development of parallel numerical implementations that scale very well to high-dimensional problems [40].

(a) Approximating the weighted residual solution of second-order stochastic ordinary differential equations

In order to solve (1.1), we introduce the following stochastic weighted residual form

$$\text{Find } \mathbf{u}(\cdot, t) \in U \text{ such that } \langle \mathbf{v}, \mathbf{M}(\boldsymbol{\xi})\ddot{\mathbf{u}} + \mathbf{K}(\boldsymbol{\xi})\,\mathbf{u} + \mathbf{C}(\boldsymbol{\xi})\dot{\mathbf{u}} - \mathbf{f}(\boldsymbol{\xi}, t)\rangle = 0, \quad \forall\, \mathbf{v} \in V, \tag{3.1}$$

where U and V denote the trial and test spaces, respectively. The inner product $\langle \cdot, \cdot \rangle$ is defined as

$$\langle \mathbf{w_1}, \mathbf{w_2} \rangle = \int_\Gamma \mathbf{w_1}(\boldsymbol{\xi})^{\mathrm{T}} \mathbf{w_2}(\boldsymbol{\xi}) \rho(\boldsymbol{\xi})\, \mathrm{d}\boldsymbol{\xi}. \tag{3.2}$$

Typically, U can be defined as the space of square integrable vectorial functions on Γ with respect to the PDF measure, i.e. $U = L^2(\Gamma)^n = \{\mathbf{w}(\boldsymbol{\xi}) \in \mathbb{R}^n, \int_\Gamma \mathbf{w}(\boldsymbol{\xi})^{\mathrm{T}} \mathbf{w}(\boldsymbol{\xi}) \rho(\boldsymbol{\xi})\, \mathrm{d}\boldsymbol{\xi} < +\infty\}$. To approximate the solution using an anchored ANOVA decomposition, the space of trial functions denoted by U_{ANOVA} can be defined as follows [40]:

$$U_{\mathrm{ANOVA}} = \mathcal{V}^n_{\boldsymbol{\xi},0} \oplus \left(\bigoplus_{j_1=1}^{N} \mathcal{V}^n_{\boldsymbol{\xi},j_1} \right) \oplus \left(\bigoplus_{j_1<j_2}^{N} \mathcal{V}^n_{\boldsymbol{\xi},j_1 j_2} \right) \oplus \cdots \oplus \mathcal{V}^n_{\boldsymbol{\xi},j_1 j_2 \cdots j_N}, \tag{3.3}$$

where the subspaces $\mathcal{V}^n_{\boldsymbol{\xi},0}$, $\mathcal{V}^n_{\boldsymbol{\xi},j_1}$, $\mathcal{V}^n_{\boldsymbol{\xi},j_1j_2}$ ... are defined as

$$\left.\begin{aligned}
&\mathcal{V}^n_{\boldsymbol{\xi},0} = \mathbf{1}_1 \otimes \cdots \otimes \mathbf{1}_N = \{\mathbf{w} \in \mathbb{R}^n\},\\
&\mathcal{V}^n_{\boldsymbol{\xi},j_1} = \mathbf{1}_1 \otimes \cdots \otimes \mathcal{W}_{\xi,j_1} \otimes \cdots \otimes \mathbf{1}_N = \left\{\mathbf{w}(\xi_{j_1}) \in \mathbb{R}^n, \int_{\Gamma_{j_1}} \mathbf{w}(\xi_{j_1})\, \mathrm{d}\mu_{j_1}(\xi_{j_1}) = 0\right\}\\
\text{and}\quad &\mathcal{V}^n_{\boldsymbol{\xi},j_1j_2} = \mathbf{1}_1 \otimes \cdots \otimes \mathcal{W}_{\xi,j_1} \otimes \cdots \otimes \mathcal{W}_{\xi,j_2} \otimes \cdots \otimes \mathbf{1}_N\\
&\qquad = \left\{\mathbf{w}(\xi_{j_1},\xi_{j_2}) \in \mathbb{R}^n, \int_{\Gamma_{j_1}}\int_{\Gamma_{j_2}} \mathbf{w}(\xi_{j_1},\xi_{j_2})\, \mathrm{d}\mu_{j_1}(\xi_{j_1})\, \mathrm{d}\mu_{j_2}(\xi_{j_2}) = 0\right\},
\end{aligned}\right\} \tag{3.4}$$

and so on. $\mathbf{1}_j$ spans constant functions with respect to the jth coordinate ξ_j and $\mathcal{W}_{\xi,j} = \{\mathbf{w} : \Gamma_j \to \mathbb{R}^n, \int_{\Gamma_j} \mathbf{w}(\xi_j)\, \mathrm{d}\mu_j(\xi_j) = \mathbf{w}(\xi_j^a) = 0\}$.

In practical computations, we shall use the following Lth-order ANOVA space

$$U^L_{\mathrm{ANOVA}} = \mathcal{V}^n_{\boldsymbol{\xi},0} \oplus \left(\bigoplus_{j_1=1}^{N} \mathcal{V}^n_{\boldsymbol{\xi},j_1}\right) \oplus \left(\bigoplus_{j_1<j_2}^{N} \mathcal{V}^n_{\boldsymbol{\xi},j_1j_2}\right) \oplus \cdots \oplus \left(\bigoplus_{j_1<\cdots<j_L}^{N} \mathcal{V}^n_{\boldsymbol{\xi},j_1\cdots j_L}\right) \tag{3.5}$$

instead of the full ANOVA expansion in (3.3). The test space V that we shall use was originally proposed in reference [40] in the context of parabolic SPDEs. The main difference compared with reference [40] is that because we are dealing with SODEs, the trial and test spaces do not depend on spatial coordinates. The space of test functions corresponding to the Lth-order truncated ANOVA decomposition is defined as

$$V^L = V_0 \oplus \left(\bigoplus_{j_1=1}^{N} V_{j_1}\right) \oplus \left(\bigoplus_{j_1<j_2}^{N} V_{j_1j_2}\right) \oplus \cdots \oplus \left(\bigoplus_{j_1<\cdots<j_L}^{N} V_{j_1\cdots j_L}\right), \tag{3.6}$$

with

$$\left.\begin{aligned}
&V_0 = \{\mathbf{w}\delta(\boldsymbol{\xi} - \boldsymbol{\xi}^{\mathrm{a}}), \mathbf{w} \in \mathbb{R}^n, \boldsymbol{\xi}^{\mathrm{a}} \in \Gamma\}, \quad \text{where } \delta(\boldsymbol{\xi} - \boldsymbol{\xi}^{\mathrm{a}}) = \prod_{i=1}^{N} \delta(\xi_i - \xi_i^a),\\
&V_{j_1} = \left\{\mathbf{w}(\xi_{j_1}) \prod_{i\neq j_1}^{N} \delta(\xi_i - \xi_i^a), \mathbf{w} \in L^2(\Gamma_{j_1})^n, \xi_i^a \in \Gamma_i\right\}\\
&\quad\vdots\\
\text{and}\quad &V_{j_1\cdots j_L} = \left\{\mathbf{w}(\xi_{j_1}\cdots\xi_{j_L}) \prod_{i\notin I_L}^{N} \delta(\xi_i - \xi_i^a), \mathbf{w} \in L^2(\Gamma_{j_1}\times\cdots\times\Gamma_{j_L})^n, \xi_i^a \in \Gamma_i, I_L = \{j_1, j_2, \ldots, j_L\}\right\},
\end{aligned}\right\} \tag{3.7}$$

In summary, when using the Lth-order truncated ANOVA approximation (2.2) for the solution of the weighted residual form (3.1), the resulting (Petrov–Galerkin) weighted residual form can be stated as

$$\text{Find } \mathbf{u}^L(\cdot,t) \in U^L_{\mathrm{ANOVA}} \text{ such that } \langle \mathbf{v}, \mathbf{M}(\boldsymbol{\xi})\ddot{\mathbf{u}}^L + \mathbf{K}(\boldsymbol{\xi})\mathbf{u}^L + \mathbf{C}(\boldsymbol{\xi})\dot{\mathbf{u}}^L - \mathbf{f}(\boldsymbol{\xi},t)\rangle = 0, \quad \forall\, \mathbf{v} \in V^L, \tag{3.8}$$

where U^L_{ANOVA}, V^L are defined by (3.5) and (3.6), respectively. Initial conditions for $\mathbf{u}^L$ and $\dot{\mathbf{u}}^L$ can be expressed in terms of $\mathbf{Z}_0$ and $\mathbf{Z}_1$ evaluated at the anchor point using (1.2), (2.6) and (2.7) as follows

$$\mathbf{u}^L(\boldsymbol{\xi},0) = \mathbf{Z}_0(\boldsymbol{\xi}^{\mathrm{a}}) + \sum_{j_1=1}^{N} (\mathbf{Z}_0(\boldsymbol{\xi}^{\mathrm{a}}_{j_1}) - \mathbf{Z}_0(\boldsymbol{\xi}^{\mathrm{a}})) + \cdots \tag{3.9}$$

and

$$\dot{\mathbf{u}}^L(\boldsymbol{\xi},0)=\mathbf{Z}_1(\boldsymbol{\xi}^{\mathrm{a}})+\sum_{j_1=1}^{N}(\mathbf{Z}_1(\boldsymbol{\xi}^{\mathrm{a}}_{j_1})-\mathbf{Z}_1(\boldsymbol{\xi}^{\mathrm{a}}))+\cdots \tag{3.10}$$

Next, we shall show that using an Lth-order anchored functional ANOVA decomposition of $\mathbf{u}(\boldsymbol{\xi},t)$ along with the test space defined earlier leads to a system of decoupled low-dimensional subproblems.

Theorem 3.1. *Consider the Lth-order truncated anchored ANOVA approximation $\mathbf{u}^L$ for the solution of the weighted residual form (3.8). Let $\mathbf{u}^0,\mathbf{u}^{j_1},\ldots,\mathbf{u}^{j_1\cdots j_L}$ be the component functions of the anchored ANOVA decomposition (2.2) that are subject to the null integral constraints (2.8). If the test functions are chosen from the space V^L defined in (3.6), then the zero-order component function $\mathbf{u}^0$ satisfies the deterministic system of ODEs*

$$\mathbf{M}(\boldsymbol{\xi}^{\mathrm{a}})\ddot{\mathbf{u}}^0+\mathbf{K}(\boldsymbol{\xi}^{\mathrm{a}})\mathbf{u}^0+\mathbf{C}(\boldsymbol{\xi}^{\mathrm{a}})\dot{\mathbf{u}}^0=\mathbf{f}(\boldsymbol{\xi}^{\mathrm{a}},t), \tag{3.11}$$

with the initial conditions $\mathbf{u}^0(0)=\mathbf{Z}_0(\boldsymbol{\xi}^{\mathrm{a}})$ and $\dot{\mathbf{u}}^0(0)=\mathbf{Z}_1(\boldsymbol{\xi}^{\mathrm{a}})$, where $\mathbf{Z}_0,\mathbf{Z}_1$ are defined in (1.2).

The higher-order ANOVA component functions $\mathbf{u}^{j_1\cdots j_k},k=1,2,\ldots,L$, are given by

$$\mathbf{u}^{j_1\cdots j_k}=\tilde{\mathbf{u}}^{j_1\cdots j_k}-\mathbf{u}^0-\sum_{l_1\in I_k}\mathbf{u}^{l_1}-\sum_{l_1<l_2,l_i\in I_k}\mathbf{u}^{l_1l_2}-\cdots-\sum_{l_1<l_2\cdots<l_{k-1},l_i\in I_k}\mathbf{u}^{l_1l_2\cdots l_{k-1}}, \tag{3.12}$$

where $I_k=\{j_1,j_2,\ldots,j_k\}$, and the auxiliary variable $\tilde{\mathbf{u}}^{j_1\cdots j_k}$ is the solution of the following low-dimensional system of SODEs (with k random variables)

$$\mathbf{M}(\boldsymbol{\xi}^{\mathrm{a}}_{j_1\cdots j_k})\ddot{\tilde{\mathbf{u}}}^{j_1\cdots j_k}+\mathbf{K}(\boldsymbol{\xi}^{\mathrm{a}}_{j_1\cdots j_k})\tilde{\mathbf{u}}^{j_1\cdots j_k}+\mathbf{C}(\boldsymbol{\xi}^{\mathrm{a}}_{j_1\cdots j_k})\dot{\tilde{\mathbf{u}}}^{j_1\cdots j_k}=\mathbf{f}(\boldsymbol{\xi}^{\mathrm{a}}_{j_1\cdots j_k},t), \tag{3.13}$$

with the initial conditions $\tilde{\mathbf{u}}^{j_1\cdots j_k}(\xi_{j_1},\ldots,\xi_{j_k},0)=\mathbf{Z}_0(\boldsymbol{\xi}^{\mathrm{a}}_{j_1\cdots j_k})$ and $\dot{\tilde{\mathbf{u}}}^{j_1\cdots j_k}(\xi_{j_1},\ldots,\xi_{j_k},0)=\mathbf{Z}_1(\boldsymbol{\xi}^{\mathrm{a}}_{j_1\cdots j_k})$.

Proof. The proof uses ideas from theorem 1 in reference [40], which presents a similar result for parabolic SPDEs. For simplicity of notation, we first rewrite (3.8) in the compact form

$$\text{Find}\ \ \mathbf{u}^L(\cdot,t)\in U^L_{\mathrm{ANOVA}}\ \text{such that}\ \langle\mathbf{v},a(\mathbf{u}^L,\dot{\mathbf{u}}^L,\ddot{\mathbf{u}}^L;\boldsymbol{\xi})-\mathbf{f}(\boldsymbol{\xi},t)\rangle=0,\quad\forall\,\mathbf{v}\in V^L, \tag{3.14}$$

where $a(\mathbf{u}^L,\dot{\mathbf{u}}^L,\ddot{\mathbf{u}}^L;\boldsymbol{\xi})=\mathbf{M}(\boldsymbol{\xi})\ddot{\mathbf{u}}^L+\mathbf{K}(\boldsymbol{\xi})\,\mathbf{u}^L+\mathbf{C}(\boldsymbol{\xi})\dot{\mathbf{u}}^L$. Expanding $\mathbf{u}^L$ and by definition of a, we have

$$a(\mathbf{u}^L,\dot{\mathbf{u}}^L,\ddot{\mathbf{u}}^L;\boldsymbol{\xi})=a(\mathbf{u}^0,\dot{\mathbf{u}}^0,\ddot{\mathbf{u}}^0;\boldsymbol{\xi})+\sum_{k=1}^{L}\sum_{j_1<\cdots<j_k}^{N}a(\mathbf{u}^{j_1\cdots j_k},\dot{\mathbf{u}}^{j_1\cdots j_k},\ddot{\mathbf{u}}^{j_1\cdots j_k};\boldsymbol{\xi}). \tag{3.15}$$

Hence, the weighted residual form (3.14) can be written as

$$\left\langle\mathbf{v},a(\mathbf{u}^0,\dot{\mathbf{u}}^0,\ddot{\mathbf{u}}^0;\boldsymbol{\xi})\right\rangle+\sum_{k=1}^{L}\sum_{j_1<\cdots<j_k}^{N}\left\langle\mathbf{v},a(\mathbf{u}^{j_1\cdots j_k},\dot{\mathbf{u}}^{j_1\cdots j_k},\ddot{\mathbf{u}}^{j_1\cdots j_k};\boldsymbol{\xi})\right\rangle=\langle\mathbf{v},\mathbf{f}(\boldsymbol{\xi},t)\rangle,\quad\forall\,\mathbf{v}\in V^L. \tag{3.16}$$

To prove (3.11), we consider test functions $\mathbf{v}\in V^L\cap V_0=V_0$ of the form $\mathbf{v}(\boldsymbol{\xi})=\mathbf{w}\delta(\boldsymbol{\xi}-\boldsymbol{\xi}^{\mathrm{a}})$, with deterministic vectors $\mathbf{w}\in\mathbb{R}^n$. Because the ANOVA component functions satisfy the null integral property (2.8), we have $\mathbf{u}^{j_1\cdots j_k}|_{\boldsymbol{\xi}=\boldsymbol{\xi}^{\mathrm{a}}}=0,\forall\,k\geq1$ and similarly $\dot{\mathbf{u}}^{j_1\cdots j_k}|_{\boldsymbol{\xi}=\boldsymbol{\xi}^{\mathrm{a}}}=0,\ddot{\mathbf{u}}^{j_1\cdots j_k}|_{\boldsymbol{\xi}=\boldsymbol{\xi}^{\mathrm{a}}}=0,\forall\,k\geq1$. As a result, (3.16) becomes the deterministic weighted residual equation

$$\mathbf{w}^{\mathrm{T}}(a(\mathbf{u}^0,\dot{\mathbf{u}}^0,\ddot{\mathbf{u}}^0;\boldsymbol{\xi}^{\mathrm{a}})-\mathbf{f}(\boldsymbol{\xi}^{\mathrm{a}},t))=0,\quad\forall\,\mathbf{w}\in\mathbb{R}^n, \tag{3.17}$$

which implies $a(\mathbf{u}^0,\dot{\mathbf{u}}^0,\ddot{\mathbf{u}}^0;\boldsymbol{\xi}^{\mathrm{a}})=\mathbf{f}(\boldsymbol{\xi}^{\mathrm{a}},t)$, i.e. equation (3.11). We shall next consider test-functions $\mathbf{v}\in V^L\cap V_{j_1\cdots j_k}=V_{j_1\cdots j_k}$ that can be written as $\mathbf{v}(\boldsymbol{\xi})=\mathbf{w}(\xi_{j_1},\ldots,\xi_{j_k})\prod_{i\notin I_k}^{N}\delta(\xi_i-\xi_i^a)$, with $I_k=$

$\{j_1,\dots,j_k\}$, $\mathbf{w}\in L^2(\Gamma_{j_1}\times\cdots\times\Gamma_{j_k})^n$. We expand the first term in (3.16) as

$$\left\langle \mathbf{v}, a\left(\mathbf{u}^0,\dot{\mathbf{u}}^0,\ddot{\mathbf{u}}^0;\boldsymbol{\xi}\right)\right\rangle = c_{j_1\cdots j_k}\int_{\Gamma_{j_1}\times\cdots\times\Gamma_{j_k}} \mathbf{w}^{\mathrm{T}} a\left(\mathbf{u}^0,\dot{\mathbf{u}}^0,\ddot{\mathbf{u}}^0;\boldsymbol{\xi}^{\mathrm{a}}_{j_1\cdots j_k}\right)\prod_{i\in I_k}\rho_i(\xi_i)\,\mathrm{d}\xi_{j_1}\cdots\mathrm{d}\xi_{j_k}, \tag{3.18}$$

with $c_{j_1\cdots j_k}=\prod_{i\notin I_k}\rho_i(\xi_i^a)>0$. The first-order terms in (3.16) can be written as

$$\sum_{j_1'=1}^{N}\left\langle v, a\left(\mathbf{u}^{j_1'},\dot{\mathbf{u}}^{j_1'},\ddot{\mathbf{u}}^{j_1'};\boldsymbol{\xi}\right)\right\rangle = c_{j_1\cdots j_k}\sum_{j_1'=1}^{N}\int_{\Gamma_{j_1}\times\cdots\times\Gamma_{j_k}} \mathbf{w}^{\mathrm{T}} a\left(\mathbf{u}^{j_1'},\dot{\mathbf{u}}^{j_1'},\ddot{\mathbf{u}}^{j_1'};\boldsymbol{\xi}^{\mathrm{a}}_{j_1\cdots j_k}\right)\prod_{i\in I_k}\rho_i(\xi_i)\,\mathrm{d}\xi_{j_1}\cdots\mathrm{d}\xi_{j_k}. \tag{3.19}$$

From the null integral constraints (2.8), we have $\mathbf{u}^{j_1'}|_{\boldsymbol{\xi}^{\mathrm{a}}_{j_1\cdots j_k}}=0$ for $j_1'\notin I_k$, $\mathbf{u}^{j_1'}|_{\boldsymbol{\xi}^{\mathrm{a}}_{j_1\cdots j_k}}=\mathbf{u}^{j_1'}$ for $j_1'\in I_k$, and similar conditions hold for the derivatives $\dot{\mathbf{u}}^{j_1'}$ and $\ddot{\mathbf{u}}^{j_1'}$. Hence, (3.19) reduces to the following summation with k terms:

$$c_{j_1\cdots j_k}\sum_{l_1\in I_k}\int_{\Gamma_{j_1}\times\cdots\times\Gamma_{j_k}} \mathbf{w}^{\mathrm{T}} a\left(\mathbf{u}^{l_1},\dot{\mathbf{u}}^{l_1},\ddot{\mathbf{u}}^{l_1};\boldsymbol{\xi}^{\mathrm{a}}_{j_1\cdots j_k}\right)\prod_{i\in I_k}\rho_i(\xi_i)\,\mathrm{d}\xi_{j_1}\cdots\mathrm{d}\xi_{j_k}. \tag{3.20}$$

Similarly, the second-order terms in (3.16) are given by

$$\begin{aligned}&\sum_{j_1'<j_2'}^{N}\left\langle v, a\left(\mathbf{u}^{j_1'j_2'},\dot{\mathbf{u}}^{j_1'j_2'},\ddot{\mathbf{u}}^{j_1'j_2'};\boldsymbol{\xi}\right)\right\rangle\\ &= c_{j_1\cdots j_k}\sum_{j_1'<j_2'}^{N}\int_{\Gamma_{j_1}\times\cdots\times\Gamma_{j_k}} \mathbf{w}^{\mathrm{T}} a\left(\mathbf{u}^{j_1'j_2'},\dot{\mathbf{u}}^{j_1'j_2'},\ddot{\mathbf{u}}^{j_1'j_2'};\boldsymbol{\xi}^{\mathrm{a}}_{j_1\cdots j_k}\right)\prod_{i\in I_k}\rho_i(\xi_i)\,\mathrm{d}\xi_{j_1}\cdots\mathrm{d}\xi_{j_k},\end{aligned} \tag{3.21}$$

which simplify to the following summation with $k(k-1)/2$ terms

$$c_{j_1\cdots j_k}\sum_{l_1<l_2,l_i\in I_k}\int_{\Gamma_{j_1}\times\cdots\times\Gamma_{j_k}} \mathbf{w}^{\mathrm{T}} a\left(\mathbf{u}^{l_1l_2},\dot{\mathbf{u}}^{l_1l_2},\ddot{\mathbf{u}}^{l_1l_2};\boldsymbol{\xi}^{\mathrm{a}}_{j_1\cdots j_k}\right)\prod_{i\in I_k}\rho_i(\xi_i)\,\mathrm{d}\xi_{j_1}\cdots\mathrm{d}\xi_{j_k}, \tag{3.22}$$

because the null integral constraints (2.8) lead to the conditions: $\mathbf{u}^{j_1'j_2'}|_{\boldsymbol{\xi}^{\mathrm{a}}_{j_1\cdots j_k}}=0$ for $j_1'\notin I_k$ or $j_2'\notin I_k$, $\mathbf{u}^{j_1'j_2'}|_{\boldsymbol{\xi}^{\mathrm{a}}_{j_1\cdots j_k}}=\mathbf{u}^{j_1'j_2'}$ for $j_1',j_2'\in I_k$ (the same conditions hold for the derivatives $\dot{\mathbf{u}}^{j_1'j_2'}$ and $\ddot{\mathbf{u}}^{j_1'j_2'}$). Similar arguments can be used when considering higher-order terms in (3.16).

Gathering all the terms obtained by expanding (3.16) such as (3.18), (3.20) and (3.22), using the fact that $c_{j_1\cdots j_k}\neq 0$ and introducing the auxiliary variable $\tilde{\mathbf{u}}^{j_1\cdots j_k}$ defined in (3.12), we recover the following low-dimensional stochastic-weighted residual form:

Find $\tilde{\mathbf{u}}^{j_1\cdots j_k}\in L^2(\Gamma_{j_1}\times\cdots\times\Gamma_{j_k})^n$ such that

$$\left\langle \mathbf{w}, a\left(\tilde{\mathbf{u}}^{j_1\cdots j_k},\dot{\tilde{\mathbf{u}}}^{j_1\cdots j_k},\ddot{\tilde{\mathbf{u}}}^{j_1\cdots j_k};\boldsymbol{\xi}^{\mathrm{a}}_{j_1\cdots j_k}\right)-\mathbf{f}\left(\boldsymbol{\xi}^{\mathrm{a}}_{j_1\cdots j_k},t\right)\right\rangle=0,\quad \forall\,\mathbf{w}\in L^2(\Gamma_{j_1}\times\cdots\times\Gamma_{j_k})^n, \tag{3.23}$$

which implies the strong form (3.13). The initial conditions, for $\mathbf{u}^0$, $\dot{\mathbf{u}}^0$ and $\tilde{\mathbf{u}}^{j_1\cdots j_k}$, $\dot{\tilde{\mathbf{u}}}^{j_1\cdots j_k}$, $k=1,\dots,L$, follow from the combination of (2.6), (2.7), (3.12) and (1.2). For example, we have

$$\mathbf{u}^0(0)=\mathbf{u}(\boldsymbol{\xi}^{\mathrm{a}},0)=\mathbf{Z}_0(\boldsymbol{\xi}^{\mathrm{a}}), \tag{3.24}$$

$$\dot{\mathbf{u}}^0(0)=\dot{\mathbf{u}}(\boldsymbol{\xi}^{\mathrm{a}},0)=\mathbf{Z}_1(\boldsymbol{\xi}^{\mathrm{a}}), \tag{3.25}$$

$$\tilde{\mathbf{u}}^{j_1}(\xi_{j_1},0)=\mathbf{u}^{j_1}(\xi_{j_1},0)+\mathbf{u}^0(0)=\mathbf{u}(\boldsymbol{\xi}^{\mathrm{a}}_{j_1},0)-\mathbf{u}^0(0)+\mathbf{u}^0(0)=\mathbf{Z}_0(\boldsymbol{\xi}^{\mathrm{a}}_{j_1}) \tag{3.26}$$

and

$$\dot{\tilde{\mathbf{u}}}^{j_1}(\xi_{j_1},0)=\dot{\mathbf{u}}^{j_1}(\xi_{j_1},0)+\dot{\mathbf{u}}^0(0)=\dot{\mathbf{u}}(\boldsymbol{\xi}^{\mathrm{a}}_{j_1},0)-\dot{\mathbf{u}}^0(0)+\dot{\mathbf{u}}^0(0)=\mathbf{Z}_1(\boldsymbol{\xi}^{\mathrm{a}}_{j_1}). \tag{3.27}$$

This completes the proof. ■

It is worth noting that the low-dimensional stochastic subproblems governing the auxiliary variables $\tilde{\mathbf{u}}^{j_1\cdots j_k}$, $k=1,2,\dots,L$, can be solved in parallel, independently of each other. After solving the subproblems (3.13) in parallel, the ANOVA component functions can be calculated using (3.12). This step ensures that the component functions $\mathbf{u}^{j_1},\mathbf{u}^{j_2},\dots,\mathbf{u}^{j_1\cdots j_L}$ are orthogonal with respect to the Dirac product measure (2.5) by construction. As an example, consider the first-order

component function $\mathbf{u}^{j_1}(\xi_{j_1},t)=\tilde{\mathbf{u}}^{j_1}(\xi_{j_1},t)-\mathbf{u}^0(t)$. From (2.6), we know that $\mathbf{u}^{j_1}(\xi_{j_1},t)=\mathbf{u}(\boldsymbol{\xi}^{\mathrm{a}}_{j_1},t)-\mathbf{u}^0(t)$, which implies the null integral condition $\mathbf{u}^{j_1}|_{\xi_{j_1}=\xi^a_{j_1}}=0$. On the other hand, because $\tilde{\mathbf{u}}^{j_1}$ satisfies the weighted residual form

$$\left\langle \mathbf{v}, a\left(\tilde{\mathbf{u}}^{j_1},\dot{\tilde{\mathbf{u}}}^{j_1},\ddot{\tilde{\mathbf{u}}}^{j_1};\boldsymbol{\xi}^{\mathrm{a}}_{j_1}\right)-\mathbf{f}\left(\boldsymbol{\xi}^{\mathrm{a}}_{j_1},t\right)\right\rangle=0,\quad \forall\,\mathbf{v}\in L^2(\Gamma_{j_1})^n, \tag{3.28}$$

we formally deduce that $\tilde{\mathbf{u}}^{j_1}$ coincides with $\mathbf{u}(\boldsymbol{\xi}^{\mathrm{a}}_{j_1},t)$. Hence, the component function $\mathbf{u}^{j_1}$ recombined using (3.12) satisfies the null integral constraint. Finally, the approximate solution $\mathbf{u}^L$ can be post-processed for its statistical moments or other metrics of interest (see §3*b*(ii) for more details). This completes the derivation of the AAPG scheme when considering SODEs of the form (1.1).

(b) Computational and implementation aspects

Here, we outline how the subproblems (3.13) arising in the AAPG scheme can be solved using gPC-based stochastic Galerkin schemes and how these solutions can be post-processed to calculate the mean and variance of the response approximation.

(i) Solution of low-dimensional subproblems

The low-dimensional subproblems (3.13) can be solved using the classical gPC method [17]. First, the random matrices $\mathbf{M}(\boldsymbol{\xi}),\mathbf{K}(\boldsymbol{\xi}),\mathbf{C}(\boldsymbol{\xi})$ and the random vector $\mathbf{f}(\boldsymbol{\xi},t)$ are expanded using gPC basis functions as follows

$$\mathbf{M}(\boldsymbol{\xi})\approx\sum_{m=0}^{N_M}\mathbf{M}_m\varphi_m(\boldsymbol{\xi}),\quad \mathbf{K}(\boldsymbol{\xi})\approx\sum_{m=0}^{N_K}\mathbf{K}_m\varphi_m(\boldsymbol{\xi}),\quad \mathbf{C}(\boldsymbol{\xi})\approx\sum_{m=0}^{N_C}\mathbf{C}_m\varphi_m(\boldsymbol{\xi}), \tag{3.29}$$

with $\mathbf{M}_m,\mathbf{K}_m,\mathbf{C}_m\in\mathbb{R}^{n\times n}$, and $\mathbf{f}(\boldsymbol{\xi},t)\approx\sum_{m=0}^{N_f}\mathbf{f}_m(t)\varphi_m(\boldsymbol{\xi})$ with $\mathbf{f}_m(t)\in\mathbb{R}^n$. The orthonormal gPC basis functions are chosen from the Askey family [18].

The gPC expansion of the solution of each subproblem (3.13), $\tilde{\mathbf{u}}^{j_1\cdots j_k}$, can be written as follows:

$$\tilde{\mathbf{u}}^{j_1\cdots j_k}\approx\hat{\tilde{\mathbf{u}}}^{j_1\cdots j_k}=\sum_{i=0}^{P_k}\boldsymbol{\beta}_i^{j_1\cdots j_k}(t)\varphi_i(\xi_{j_1},\ldots,\xi_{j_k}), \tag{3.30}$$

where $\boldsymbol{\beta}_i^{j_1\cdots j_k}\in\mathbb{R}^n$, $i=0,1,\ldots,P_k$, are undetermined expansion coefficients. The number of terms in the expansion (3.30) is a function of the number of active random variables (k) in the subproblem and the gPC expansion order (p), i.e. $P_k+1=(k+p)!/k!p!$ It can be seen that P_k increases rapidly with respect to k, especially when high gPC expansion order p is required to ensure good accuracy. However, this is not an issue in the AAPG formulation, because k is less than or equal to the functional ANOVA expansion order L, which in turn is significantly smaller than the total number of random variables, N.

Applying the stochastic Galerkin projection scheme [17] to the subproblem (3.13)

$$\mathbf{M}(\boldsymbol{\xi}^{\mathrm{a}}_{j_1\cdots j_k})\hat{\ddot{\tilde{\mathbf{u}}}}^{j_1\cdots j_k}+\mathbf{K}(\boldsymbol{\xi}^{\mathrm{a}}_{j_1\cdots j_k})\hat{\dot{\tilde{\mathbf{u}}}}^{j_1\cdots j_k}+\mathbf{C}(\boldsymbol{\xi}^{\mathrm{a}}_{j_1\cdots j_k})\hat{\tilde{\mathbf{u}}}^{j_1\cdots j_k}-\mathbf{f}(\boldsymbol{\xi}^{\mathrm{a}}_{j_1\cdots j_k},t)\perp\varphi_i,\quad i=0,1,\ldots,P_k, \tag{3.31}$$

leads to a system of P_k+1 coupled deterministic ODEs which govern the coefficients $\boldsymbol{\beta}_i^{j_1\cdots j_k}$. Writing the stochastic Galerkin conditions for the initial conditions of (3.13) as

$$\hat{\tilde{\mathbf{u}}}^{j_1\cdots j_k}(\xi_{j_1}\cdots\xi_{j_k},0)-\mathbf{Z}_0(\boldsymbol{\xi}^{\mathrm{a}}_{j_1\cdots j_k})\perp\varphi_i,\quad i=0,1,\ldots,P_k \tag{3.32}$$

and

$$\hat{\dot{\tilde{\mathbf{u}}}}^{j_1\cdots j_k}(\xi_{j_1}\cdots\xi_{j_k},0)-\mathbf{Z}_1(\boldsymbol{\xi}^{\mathrm{a}}_{j_1\cdots j_k})\perp\varphi_i,\quad i=0,1,\ldots,P_k, \tag{3.33}$$

leads to the following initial conditions for the gPC expansion coefficients in (3.30)

$$\boldsymbol{\beta}_i^{j_1\cdots j_k}(0)=\langle\mathbf{Z_0}(\boldsymbol{\xi}^{\mathrm{a}}_{j_1\cdots j_k})\varphi_i\rangle,\quad i=0,1,\ldots,P_k \tag{3.34}$$

and

$$\dot{\boldsymbol{\beta}}_i^{j_1\cdots j_k}(0) = \left\langle \mathbf{Z_1}(\boldsymbol{\xi}^{\mathrm{a}}_{j_1\cdots j_k})\varphi_i \right\rangle, \quad i = 0, 1, \ldots, P_k, \tag{3.35}$$

that can be used to solve the deterministic ODEs arising from (3.31).

(ii) Post-processing for response statistics

Here, we present explicit formulae for the mean and variance of $\mathbf{u}^L$ when $L = 2$. Assuming that the low-dimensional subproblems are solved using the classical gPC Galerkin projection scheme as outlined earlier in §3b(i), the second-order ANOVA approximation can be written as

$$\mathbf{u}^L(\boldsymbol{\xi}, t) \approx \alpha_0 \mathbf{u}^0(t) + \sum_{j_1 \le j_2}^{N} \sum_{i=0}^{P_2} \boldsymbol{\lambda}_i^{j_1 j_2}(t)\varphi_i(\xi_{j_1}, \xi_{j_2}), \tag{3.36}$$

with

$$\alpha_0 = \left(1 - N + \frac{N(N-1)}{2}\right) \tag{3.37}$$

and

$$\boldsymbol{\lambda}_i^{j_1 j_2} = \begin{cases} \boldsymbol{\beta}_i^{j_1 j_2} & \text{for } j_1 < j_2, i = 0, 1, \ldots, P_2, \\ (2 - N)\boldsymbol{\beta}_{I^{-1}(i)}^{j_1} & \text{for } j_1 = j_2 \text{ and } i \in A, \\ 0 & \text{for } j_1 = j_2 \text{ and } i \notin A. \end{cases} \tag{3.38}$$

Note that for simplicity of notation, the first- and second-order gPC basis and coefficients in (3.36) are collectively written as $\varphi_i(\xi_{j_1}, \xi_{j_2})$ and $\boldsymbol{\lambda}_i^{j_1 j_2}(t)$, respectively. The mapping $i \in \{0, 1, \ldots, P_1\} \mapsto I(i) \in A \subset \{0, 1, \ldots, P_2\}$ is introduced to express the first-order gPC terms in the form of second-order gPC terms. Using (3.36), the mean and the variance of $\mathbf{u}^L$ are explicitly given by

$$\boldsymbol{\mu}_{\mathrm{AAPG}}(t) \approx \alpha_0 \mathbf{u}^0(t) + \sum_{j_1 \le j_2}^{N} \boldsymbol{\lambda}_0^{j_1 j_2}(t) \tag{3.39}$$

and

$$\boldsymbol{\sigma}^2_{\mathrm{AAPG}}(t) \approx \sum_{i=1}^{P_2} \sum_{j_1 \le j_2}^{N} \mathrm{diag}\,(\boldsymbol{\lambda}_i^{j_1 j_2}(t) \cdot (\boldsymbol{\lambda}_i^{j_1 j_2}(t))^{\mathrm{T}}). \tag{3.40}$$

Similar expressions can be derived for the statistics of the velocity and acceleration vectors.

4. Numerical studies

Numerical studies are presented for two- and three-dimensional model problems in linear stochastic structural dynamics. The Young modulus in both case studies is treated as a random field and discretized using a Karhunen–Loève (KL) expansion scheme [43].

(a) Two-dimensional beam example

Consider a cantilevered two-dimensional linear elastic beam made of aluminium with length $L = 10$ m, width $W = 1$ m, shear modulus $G = 26$ GPa, Poisson ratio $\nu = 0.35$ and mass density $\rho = 2.70 \times 10^3\ \mathrm{kg\,m^{-3}}$. We model the Young modulus of the beam as a random field with mean $E_0 = 70$ GPa. A mass proportional damping model is used in the analysis, i.e. $\mathbf{C} = \alpha_{\mathrm{dM}}\mathbf{M}$, where the constant $\alpha_{\mathrm{dM}} = 10$. The finite-element (FE) mesh used for this problem is shown in figure 1*a*, where the total number of d.f. is $n = 88$. This relatively coarse mesh is used for validating the proposed AAPG formulation (a more refined FE mesh will be used in the next example).

We study the dynamic response over the time interval $[0, T], T = 2(s)$ with zero initial conditions for the displacement and velocity. A time-dependent force of the form $\bar{f}(1 - [1 - \sin(bt)] \cdot \mathrm{e}^{-at})$ is applied to the upper right tip of the beam in the x_2-direction, where $\bar{f} = 10^5$ N. The constants a and b are used to control the amplitude and the period of the source term. In our test-case, we take $a = 3/T$, $b = 20\pi/T$. The time-dependent part of force is depicted in figure 1*b*.

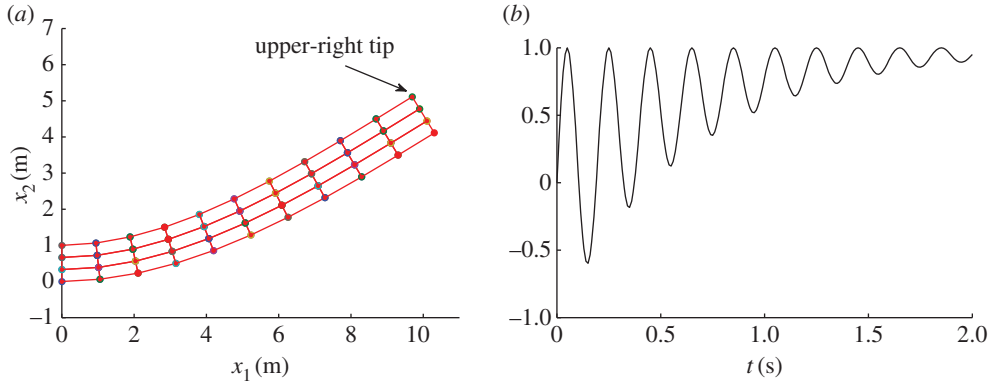

Figure 1. Two-dimensional beam clamped at one end and external force applied to its upper-right tip in the x_2-direction. (*a*) Deformed configuration of the beam at $T = 2(s)$ with displacement amplified by a factor of 10^3. (*b*) Time-dependent part of the external force with $T = 2(s)$, $a = 3/T$, $b = 20\pi/T$. (Online version in colour.)

(i) Random field discretization

In this case study, the Young modulus is modelled as a random field $E(\mathbf{x}, \omega)$, where $\mathbf{x} = (x_1, x_2)^{\mathrm{T}}$ denotes the spatial coordinates and $\omega \in \Omega$. The covariance function is chosen to be

$$C(\mathbf{x}, \mathbf{y}) = \sigma^2 \exp\left(-\frac{|x_1 - y_1|}{c_1} - \frac{|x_2 - y_2|}{c_2}\right), \tag{4.1}$$

where $\mathbf{y} = (y_1, y_2)^{\mathrm{T}}$, σ is the standard deviation of the field and c_1 and c_2 are the correlation lengths in x_1- and x_2-directions, respectively. In this test-case, we set $\sigma = 0.1$ and $c_1 = c_2 = 1$.

Various techniques exist for discretizing random fields in terms of a set of independent random variables, such as KL expansions [43] and orthogonal series [44]. In this study, we employ the KL expansion scheme for discretizing $E(\mathbf{x}, \omega)$; a detailed description of the convergence properties of this expansion scheme can be found in reference [45]. The truncated KL expansion of the random field $E(\mathbf{x}, \omega)$ can be written as

$$E(\mathbf{x}, \omega) = E_0 + \sum_{m=1}^{\infty} \xi_m(\omega) E_m(\mathbf{x}) \approx E_0 + \sum_{m=1}^{N} \xi_m(\omega) E_m(\mathbf{x}). \tag{4.2}$$

Here, $E_0 = 70\,\mathrm{GPa}$ is the mean value of $E(\mathbf{x}, \omega)$ and ξ_m are uncorrelated uniform random variables in the interval $[-1, 1]$. The spatial basis functions $E_m(\mathbf{x}), m = 1, 2, \ldots, N$ are given by $E_m(\mathbf{x}) = \sigma\sqrt{\lambda_m}\kappa_m(\mathbf{x})$, where λ_m and $\kappa_m(\mathbf{x})$ are the eigenvalues and eigenfunctions of the following Fredholm integral equation of the second kind

$$\int_D C(\mathbf{x}, \mathbf{y}) \kappa_m(\mathbf{y})\, \mathrm{d}\mathbf{y} = \lambda_m \kappa_m(\mathbf{x}), \tag{4.3}$$

where D is the spatial domain, $C(\mathbf{x}, \mathbf{y})$ is defined in (4.1) and λ_m are such that $\lambda_1 \geq \lambda_2 \geq \cdots \geq \lambda_N$. Using (4.2), the constitutive matrix can be written as

$$\mathbf{D}(\mathbf{x}, \boldsymbol{\xi}) \approx \mathbf{D}_0 + \sum_{m=1}^{N} \xi_m \mathbf{D}_m(\mathbf{x}). \tag{4.4}$$

The stochastic element stiffness matrix is given by $k^{\mathrm{e}}(\boldsymbol{\xi}) = \int_{D_{\mathrm{e}}} \mathbf{B}^{\mathrm{T}} \mathbf{D}(\mathbf{x}, \boldsymbol{\xi}) \mathbf{B}\, \mathrm{d}\mathbf{x}$, where $\mathbf{B}$ is the strain–displacement matrix and D_{e} denotes the domain of the element. Using (4.4), the stochastic element stiffness matrix can be written as $k^{\mathrm{e}}(\boldsymbol{\xi}) = k_0^{\mathrm{e}} + \sum_{m=1}^{N} \xi_m k_m^{\mathrm{e}}$, where $k_0^{\mathrm{e}} = \int_{D_{\mathrm{e}}} \mathbf{B}^{\mathrm{T}} \mathbf{D}_0 \mathbf{B}\, \mathrm{d}\mathbf{x}$ and $k_m^{\mathrm{e}} = \int_{D_{\mathrm{e}}} \mathbf{B}^{\mathrm{T}} \mathbf{D}_m \mathbf{B}\, \mathrm{d}\mathbf{x}$. Standard numerical quadrature schemes can be used to evaluate these integrals (for more details, see reference [17]). Assembling the element stiffness matrices and accounting

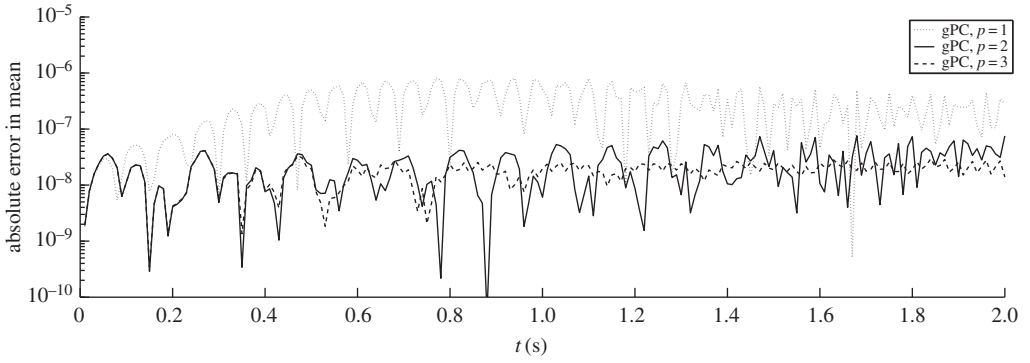

Figure 2. Two-dimensional beam test-case: absolute error in mean displacement as a function of time for gPC-based stochastic Galerkin projection schemes.

for the specified boundary conditions result in the following expansion for the global stiffness matrix

$$\mathbf{K}(\boldsymbol{\xi}) = \mathbf{K}_0 + \sum_{m=1}^{N} \xi_m \mathbf{K}_m, \tag{4.5}$$

where $\mathbf{K}_0 \in \mathbb{R}^{n\times n}, \mathbf{K}_m \in \mathbb{R}^{n\times n}$ are deterministic matrices. In the case studies considered in this work, the mass and damping matrices are assumed to be deterministic.

In the following sections, the gPC-based stochastic Galerkin projection scheme, GSD and AAPG methods are applied for solving the model problem described earlier with $N = 5$ uniform random variables. The average acceleration Newmark integration scheme [46] is chosen as the time-marching scheme for all methods. We shall compare the accuracy of different numerical schemes for approximating the statistics of the displacement component in the x_2-direction at the upper right tip of the beam (figure 1*a*). MCS with a sample size of $M = 10^6$ is used to generate benchmark results against which the accuracy of other methods are evaluated (the CPU time required by MCS is 1.96×10^5 s for this model problem).

(ii) Application of the generalized polynomial chaos projection scheme

The mean and standard deviation of solutions obtained using gPC-based stochastic Galerkin projection with gPC order $p = 1, 2, 3$ are compared with MCS results in figures 2 and 3. It can be observed that the higher-order gPC approximations are in good agreement with those obtained using MCS. The CPU time required by the gPC-based stochastic Galerkin projection scheme with $p = 1, 2, 3$ are 0.22, 3.93 and 50.33 s, respectively. It is to be noted that the computational cost will be significantly higher when the gPC expansion order is increased for systems with larger number of degrees of freedom. For example, when the gPC scheme is applied to the three-dimensional hex example later in §4b, using $p = 3$ can be computationally much more demanding. Henceforth, the gPC scheme with $p = 2$ will be used as the reference solution in the following sections when comparing the performance of different schemes.

(iii) Application of the generalized spectral decomposition scheme

We consider here a subspace iteration version of Nouy's GSD scheme [24,25] for this model problem. The GSD decomposition of the response can be written as

$$\mathbf{u}(\boldsymbol{\xi}, t) \approx \hat{\mathbf{u}}(\boldsymbol{\xi}, t) = \sum_{k=1}^{K} \lambda_k(\boldsymbol{\xi}) \boldsymbol{\phi}_k(t), \tag{4.6}$$

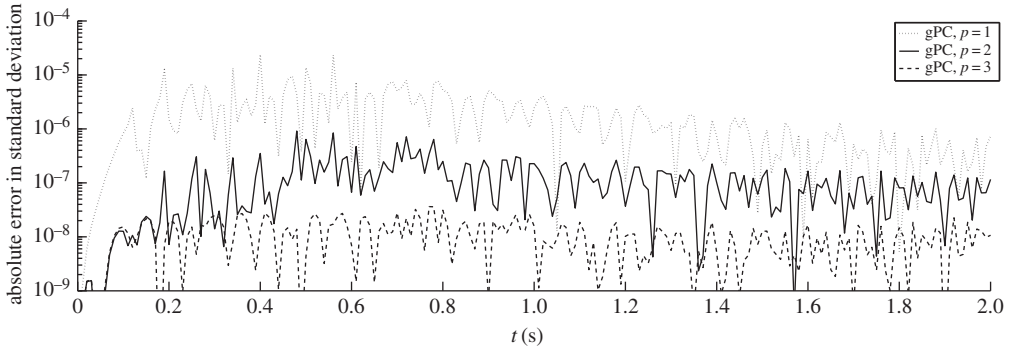

Figure 3. Two-dimensional beam test-case: absolute error in standard deviation of displacement as a function of time for gPC-based stochastic Galerkin projection schemes.

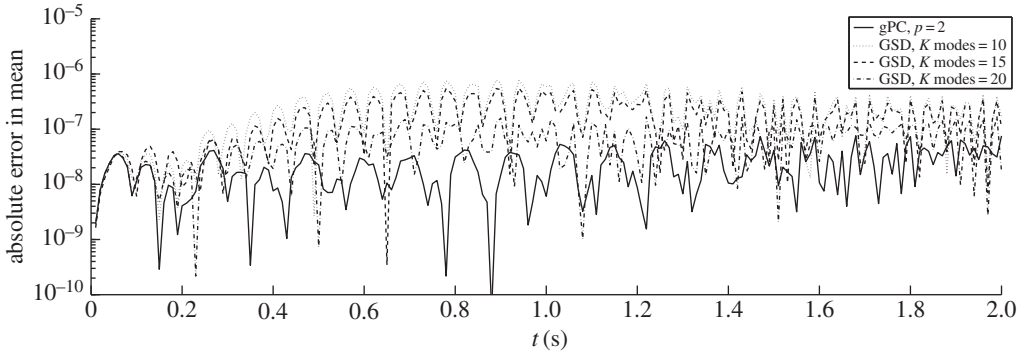

Figure 4. Two-dimensional beam test-case: absolute error in mean of displacement as a function of time for the GSD schemes with different values of K.

where $\lambda_k(\boldsymbol{\xi}), k=1,2,\ldots,K$, denote undetermined random scalars and $\boldsymbol{\phi}_k(t) \in \mathbb{R}^n$ are undetermined time-dependent vectors. Starting with an initial guess chosen randomly for $\boldsymbol{\phi}_k(t), k=1,2,\ldots,K$, the following two-step iterative procedure can be used to compute $\lambda_k(\boldsymbol{\xi})$ and $\boldsymbol{\phi}_k(t)$:

— step 1: given $\boldsymbol{\phi}_k(t)$, solve for $\lambda_k(\boldsymbol{\xi}), k=1,2,\ldots,K$. This step involves the application of the Galerkin condition $\int_0^{\mathrm{T}} \boldsymbol{\phi}_j^{\mathrm{T}}(t)\boldsymbol{R}(\hat{\mathbf{u}}(\boldsymbol{\xi},t))\,\mathrm{d}t = 0,\ j=1,2,\ldots,K$.
— step 2: given $\lambda_k(\boldsymbol{\xi})$, solve for $\boldsymbol{\phi}_k(t), k=1,2,\ldots,K$. This step involves the application of the Galerkin condition $\int_{\Gamma} \boldsymbol{R}(\hat{\mathbf{u}}(\boldsymbol{\xi},t))\lambda_j(\boldsymbol{\xi})\rho(\boldsymbol{\xi})\,\mathrm{d}\boldsymbol{\xi} = 0,\ j=1,2,\ldots,K$.

The residual error is defined as $\boldsymbol{R}(\hat{\mathbf{u}}(\boldsymbol{\xi},t)) = \mathbf{M}(\boldsymbol{\xi})\ddot{\hat{\mathbf{u}}}(\boldsymbol{\xi},t) + \mathbf{K}(\boldsymbol{\xi})\hat{\mathbf{u}}(\boldsymbol{\xi},t) + \mathbf{C}(\boldsymbol{\xi})\dot{\hat{\mathbf{u}}}(\boldsymbol{\xi},t) - \mathbf{f}(\boldsymbol{\xi},t)$, where $\hat{\mathbf{u}}$ is given by (4.6). To ensure that the expansion in (4.6) is unique, the modified Gram–Schmidt procedure is applied to orthogonalize $\lambda_k(\boldsymbol{\xi})$ and $\boldsymbol{\phi}_k(t)$ before applying steps 1 and 2, respectively.

In practice, the accuracy of the GSD method depends on the number of modes (K) and the optimal value of this user defined parameter needs to be carefully chosen to trade off between accuracy and computational efficiency. In addition, the performance of GSD method will depend as well on the stopping criterion used to terminate the iterations. In the numerical studies presented here, the GSD iterations are stopped when the difference between two successive residual norms (the residual norm being defined as $\int_0^{\mathrm{T}} \int_{\Gamma} \mathbf{R}^{\mathrm{T}}\mathbf{R}\rho(\boldsymbol{\xi})\,\mathrm{d}\boldsymbol{\xi}\,\mathrm{d}t$) is smaller than 10^{-8} or when the number of iterations reaches a maximal value (taken as 15).

The absolute error in the mean and standard deviation of the displacement component in the x_2-direction at the upper right tip of the beam with respect to the MCS results are shown in

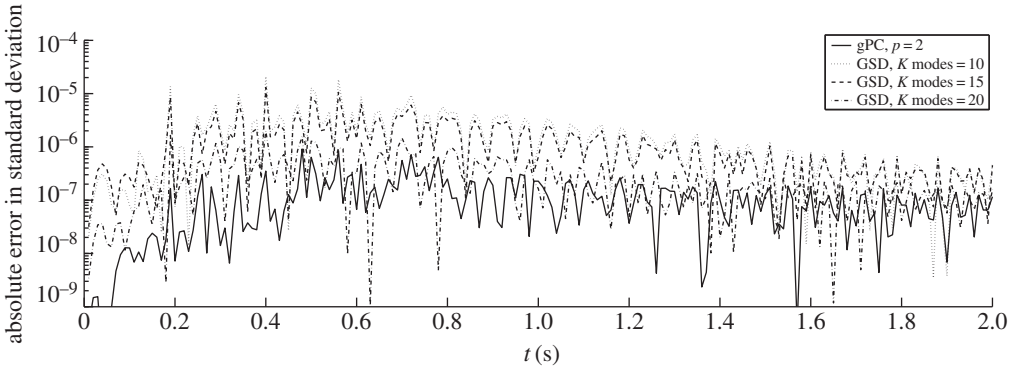

Figure 5. Two-dimensional beam test-case: absolute error in standard deviation of displacement as a function of time for the GSD schemes with different values of K.

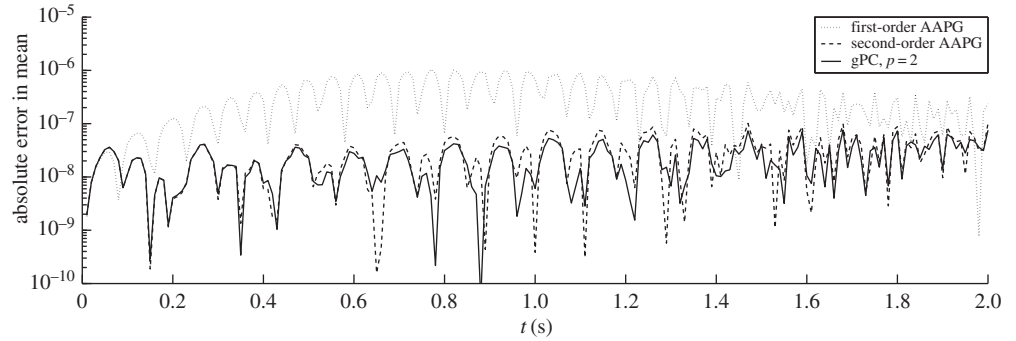

Figure 6. Two-dimensional beam test-case: absolute error in mean of displacement as a function of time for the first- and second-order AAPG schemes. Error of second-order gPC method is also included for comparison.

figures 4 and 5. The corresponding errors for the second-order gPC scheme are also included as a reference. It can be observed that approximation errors for the GSD scheme decrease when increasing the number of modes (K). When $K=20$, the accuracy of GSD is comparable to the second-order gPC method. The CPU time required by GSD with $K=10$, 15 and 20 are 215, 372 and 559 s, respectively. For this particular problem, subspace iteration version of GSD turns out to be less efficient than the second-order gPC method which required 3.93 s. This is probably a consequence of the relatively small number of d.f. ($n=88$) for this simple test-case and the termination criterion we used.

(iv) Application of the AAPG scheme

We now present results obtained using the first- and second-order AAPG schemes for this model problem, i.e. $\mathbf{u}^L$ with $L=1,2$ in (2.2). The low-dimensional subproblems of the form (3.13) are solved sequentially using a second-order gPC-based stochastic Galerkin projection scheme; see §3b(i). The anchor point $\boldsymbol{\xi}^{\mathrm{a}}$ used in (2.5) is set to $\xi_i^{\mathrm{a}}=\langle\xi_i\rangle=0,\ i=1,\ldots,N$. Because the mean and standard deviation of the response calculated using AAPG and MCS are very close to each other, they are not shown separately here. The absolute error in mean and standard deviation of the displacement at the upper right tip of the beam computed using the AAPG schemes are presented in figures 6 and 7. The errors corresponding to the second-order gPC scheme are also included as a reference.

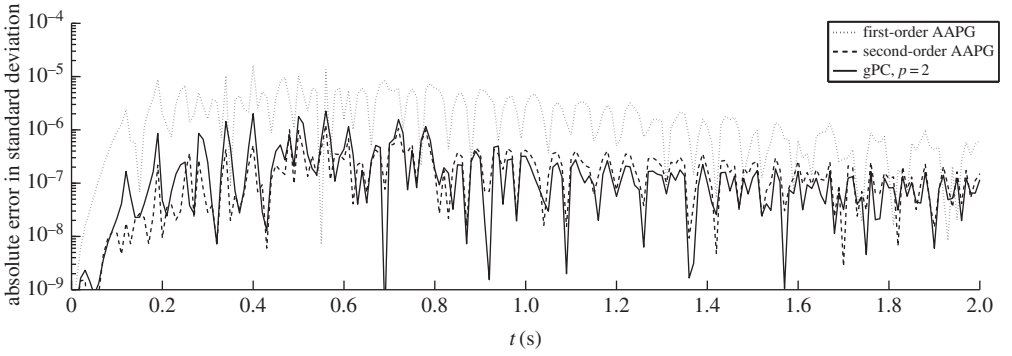

Figure 7. Two-dimensional beam test-case: absolute error in standard deviation of displacement as a function of time for the first- and second-order AAPG schemes. Error of second-order gPC method is also included for comparison.

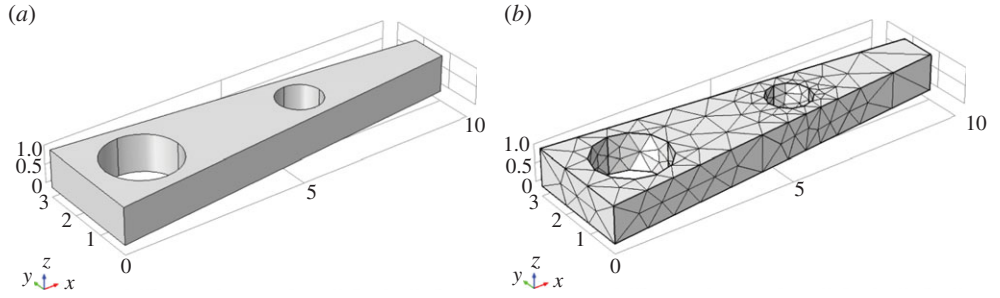

Figure 8. Hex-shaped structure with two cylinder-shaped holes. One cylinder is centred at $x = 1.5$, $y = 1.5$ with radius $r = 1$, and the other one at $x = 6$, $y = 1.5$ with radius $r = 0.6$. Both cylinders have the same height as the hex, which is 1. (Online version in colour.)

It can be seen from figures 6 and 7 that the first-order AAPG scheme has a higher level of error compared with the second-order gPC method, whereas the second-order AAPG scheme provides accuracy levels comparable to the second-order gPC method. The computational time required by the second-order AAPG scheme is 2.62 s, whereas the full second-order gPC method requires 3.93 s. It is to be noted that in our current implementation the AAPG subproblems are solved sequentially.

(b) Three-dimensional hex example

In this three-dimensional test-case, we consider a hex-shaped linear structure with two cylinder-shaped holes as shown in figure 8. Spatial discretization is carried out using second-order (10 node) tetrahedral elements leading to a total of 4446 d.f. Mass proportional damping is considered ($\mathbf{C} = 10\mathbf{M}$) and the material properties are taken to be the same as in the two-dimensional beam example (see §4a). One face of the structure is clamped at $x = 0$. A time-dependent deterministic force $\mathbf{f}(t)$ of the form considered in the previous example with net magnitude of 10^5 N is evenly applied to another face ($x = 10$) in the y-direction, with $a = 3/T$, $b = 20\pi/T$. The dynamic response over the interval $[0, T]$, $T = 1$ s, is considered with zero initial conditions for the displacement and velocity.

Similar to the two-dimensional example, the Young modulus is treated as a random field with mean value $E_0 = 70$ GPa and a covariance function of the form

$$C(\mathbf{x}, \mathbf{y}) = \sigma^2 \exp\left(-\frac{|x_1 - y_1|}{c_1} - \frac{|x_2 - y_2|}{c_2} - \frac{|x_3 - y_3|}{c_3}\right), \tag{4.7}$$

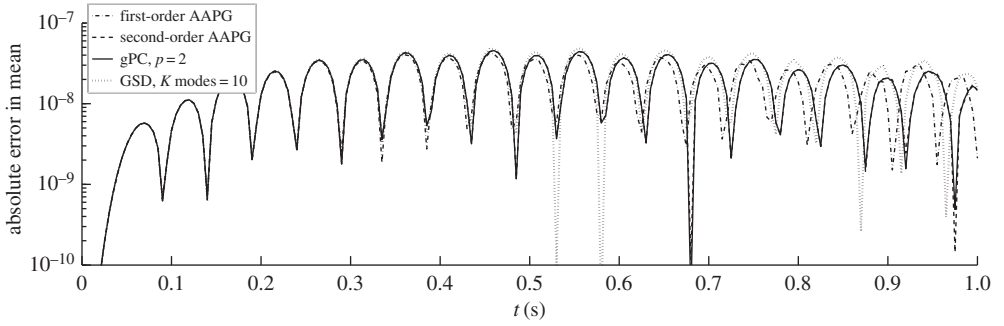

Figure 9. Three-dimensional hex test-case: absolute error in mean of displacement at node $(x, y, z) = (10, 2, 1)$ as a function of time for second-order gPC, GSD with $K = 10$ modes, first- and second-order AAPG schemes.

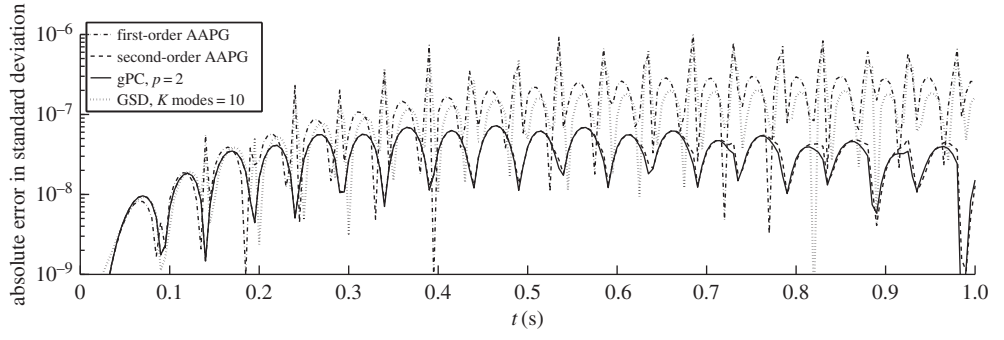

Figure 10. Three-dimensional hex test-case: absolute error in standard deviation of displacement at node $(x, y, z) = (10, 2, 1)$ as a function of time for second-order gPC, GSD with $K = 10$ modes, first- and second-order AAPG schemes.

with $\sigma = 0.1$ and $c_1 = c_2 = c_3 = 1$. The random field is discretized using the KL expansion scheme (see §4a(i)) and $N = 5$ terms are retained in the expansion. The random variables are considered to be uniformly distributed in the interval $[-1, 1]$.

Second-order gPC, GSD with $K = 10$ modes and sequential versions of first- and second-order AAPG schemes are applied to this problem. The anchor point $\boldsymbol{\xi}^a$ for AAPG schemes is taken as $\xi_i^a = \langle \xi_i \rangle = 0, i = 1, \ldots, N$. The absolute errors in the mean and standard deviation of the displacement at the node $(x, y, z) = (10, 2, 1)$ are shown in figures 9 and 10, respectively. Results obtained using MCS with sample size $M = 100\,000$ are used as reference solutions while calculating the errors. It can be seen that the error in the mean response computed using the different schemes are comparable (figure 9). By contrast, the errors in the standard deviation computed using GSD with $K = 10$ modes and first-order AAPG are one order of magnitude higher compared with second-order gPC and second-order AAPG (figure 10).

The CPU times required by the different schemes are listed in table 1. Sequential second-order AAPG turns out to be faster than second-order gPC while providing similar level of errors. For different values of K, GSD is computationally more expensive than gPC and AAPG schemes for this particular test-case. However, it is worth noting that it may be possible to speed up the GSD scheme using a different numerical procedure for estimating the component functions [26]. In addition, using another stopping criterion to terminate the GSD iterations could also lead to computational cost reductions. For this particular test-case, the second-order AAPG scheme offers the best efficiency while providing the same level of accuracy compared with the second-order gPC method.

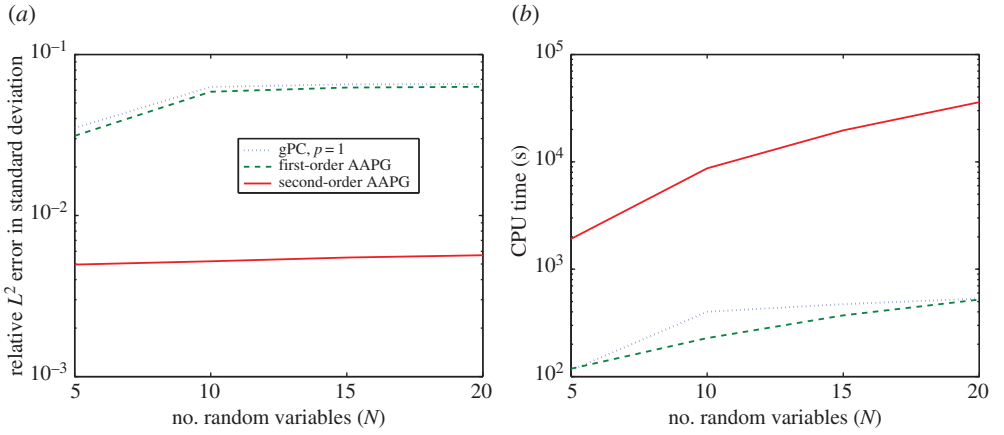

Figure 11. Performance of first- and second-order AAPG schemes as a function of the number of random variables (N). The time-averaged relative L^2 error in the response standard deviation approximation is computed as $||\sigma_{\text{AAPG}} - \sigma_{\text{MCS}}||_{L^2([0,T])}/||\sigma_{\text{MCS}}||_{L^2([0,T])}$, where the MCS solution is used as reference. First-order gPC results are also included for comparison. (Online version in colour.)

Table 1. CPU times required by different methods. Results are generated using Matlab codes on a machine with Intel i7-2600 CPU and 16 GB RAM.

	CPU time (s)
MCS, sample size $M = 10^5$	1.388×10^5
second-order gPC	3.395×10^3
GSD, $K = 5$	2.387×10^4
GSD, $K = 10$	9.582×10^4
GSD, $K = 15$	2.181×10^5
sequential second-order AAPG	1.894×10^3

We also conducted some additional numerical studies to examine the performance of the AAPG schemes when the number of random variables is increased, i.e. for $N = 5, 10, 15, 20$. Figure 11 shows the time-averaged relative error in the response variance approximation and the CPU time of the first- and second-order AAPG schemes as a function of N. Similar trends for the first-order gPC scheme are included for comparison. The computational cost and memory requirements of the second-order gPC and GSD schemes are much higher and not presented in these figures. Figure 11*a* shows that the level of L^2 error for the second-order AAPG scheme is about one order of magnitude lower than the first-order AAPG and gPC schemes. The CPU times shown in figure 11*b* are for a sequential implementation. For systems with a large number of spatial and stochastic degrees of freedom, the decoupled subproblems arising in the AAPG scheme will need to be solved in parallel to achieve further reductions in CPU time.

5. Concluding remarks

In this paper, we have proposed AAPG projection schemes for solving a class of stochastic ordinary differential equations encountered in linear stochastic structural dynamics. The main idea of the proposed formulation is to approximate the dynamic response using a Hoeffding functional ANOVA decomposition along with appropriate constraints to ensure the uniqueness of the decomposition. We showed that when the test functions in the weighted residual form are

chosen appropriately, the original high-dimensional stochastic problem can be decoupled into a sequence of low-dimensional stochastic subproblems that can be solved independently of each other.

Numerical studies on a set of linear stochastic structural dynamical systems suggest that the AAPG scheme with second-order truncation provides accuracy that is comparable to the classical gPC-based stochastic Galerkin approach and the iterative GSD scheme, while incurring lower computational cost. For large-scale systems, the AAPG projection scheme will be significantly faster compared with existing methods, because the low-dimensional subproblems arising in this scheme are decoupled and can be solved in parallel independently of each other. The AAPG projection scheme is expected to perform very well for systems where the dynamic response has a low-effective dimension (i.e. when a low-order ANOVA truncation is sufficient to capture the response statistics). Another advantage offered by the AAPG formulation is that it is a non-iterative scheme in contrast to the GSD approach. Ongoing work is focusing on parallel implementation aspects for solving high-dimensional stochastic problems with a larger number of stochastic and spatial degrees of freedom. Various other computational aspects of the proposed approach also remain to be investigated further, such as using adaptivity metrics based on Sobol sensitivity indices [36] to achieve further improvements in efficiency, decompositions with multiple anchor points and the application of AAPG schemes to nonlinear stochastic structural dynamics.

Data accessibility. Electronic supplementary material accompanies the article online.

Authors' contributions. L.G. implemented the numerical methods, carried out numerical studies and drafted the manuscript; C.A. participated in the mathematical formulation, implementation of numerical methods and manuscript preparation; P.B.N. defined and led the research and manuscript preparation.

Competing interests. We have no competing interests.

Funding. This research is supported by an NSERC Discovery Grant and the Canada Research Chairs program.

References

1. Øksendal B. 2003 *Stochastic differential equations. An introduction with applications*. 6th edn. Berlin, Germany: Springer.
2. Hurtado J, Barbat A. 1998 Monte Carlo techniques in computational stochastic mechanics. *Arch. Comput. Methods Eng.* **5**, 3–29. (doi:10.1007/BF02736747)
3. Papadrakakis M, Papadopoulos V. 1996 Robust and efficient methods for stochastic finite element analysis using Monte Carlo simulation. *Comput. Methods Appl. Mech. Eng.* **134**, 325–340. (doi:10.1016/0045-7825(95)00978-7)
4. Matthies HG, Brenner CE, Bucher CG, Guedes Soares C. 1997 Uncertainties in probabilistic numerical analysis of structures and solids-stochastic finite elements. *Struct. Saf.* **19**, 283–336. (doi:10.1016/S0167-4730(97)00013-1)
5. Manohar C, Ibrahim R. 1999 Progress in structural dynamics with stochastic parameter variations: 1987–1998. *Appl. Mech. Rev.* **52**, 177–197. (doi:10.1115/1.3098933)
6. Schuëller GI. 2001 Computational stochastic mechanics-recent advances. *Comput. Struct.* **79**, 2225–2234. (doi:10.1016/S0045-7949(01)00078-5)
7. Schuëller G, Pradlwarter H. 2009 Uncertain linear systems in dynamics: retrospective and recent developments by stochastic approaches. *Eng. Struct.* **31**, 2507–2517. (doi:10.1016/j.engstruct.2009.07.005)
8. Stefanou G. 2009 The stochastic finite element method: past, present and future. *Comput. Methods Appl. Mech. Eng.* **198**, 1031–1051. (doi:10.1016/j.cma.2008.11.007)
9. Kundu A, Adhikari S. 2014 Transient response of structural dynamic systems with parametric uncertainty. *ASCE J. Eng. Mech.* **140**, 315–331. (doi:10.1061/(ASCE)EM.1943-7889.0000643)
10. Soize C. 2005 A comprehensive overview of a non-parametric probabilistic approach of model uncertainties for predictive models in structural dynamics. *J. Sound Vib.* **288**, 623–652. (doi:10.1016/j.jsv.2005.07.009)
11. Soize C. 2005 Random matrix theory for modeling uncertainties in computational mechanics. *Comput. Methods Appl. Mech. Eng.* **194**, 1333–1366. (doi:10.1016/j.cma.2004.06.038)
12. Soize C. 2000 A nonparametric model of random uncertainties for reduced matrix models in structural dynamics. *Probab. Eng. Mech.* **15**, 277–294. (doi:10.1016/S0266-8920(99)00028-4)

13. Adhikari S. 2007 Matrix variate distributions for probabilistic structural dynamics. *AIAA J.* **45**, 1748–1762. (doi:10.2514/1.25512?journalCode=aiaaj)
14. Adhikari S. 2008 Wishart random matrices in probabilistic structural mechanics. *J. Eng. Mech.* **134**, 1029–1044. (doi:10.1061/(ASCE)0733-9399(2008)134:12(1029))
15. Moens D, Hanss M. 2011 Non-probabilistic finite element analysis for parametric uncertainty treatment in applied mechanics: recent advances. *Finite Element Anal. Des.* **47**, 4–16. (doi:10.1016/j.finel.2010.07.010)
16. Mace BR, Vandepitte DV, Lardeur P. 2011 Uncertainty in structural dynamics. *Finite Element Anal. Des.* **47**, 1–3. (doi:10.1016/j.finel.2010.07.021)
17. Ghanem R, Spanos PD. 1991 *Stochastic finite elements: a spectral approach*. New York, NY: Springer.
18. Xiu D, Karniadakis G. 2002 The Wiener–Askey polynomial chaos for stochastic differential equations. *SIAM J. Sci. Comput.* **24**, 619–644. (doi:10.1137/S1064827501387826)
19. Sarkar A, Ghanem R. 2002 Mid-frequency structural dynamics with parameter uncertainty. *Comput. Methods Appl. Mech. Eng.* **191**, 5499–5513. (doi:10.1016/S0045-7825(02)00465-6)
20. Ghanem R, Ghosh D. 2007 Efficient characterization of the random eigenvalue problem in a polynomial chaos decomposition. *Int. J. Numer. Methods Eng.* **72**, 486–504. (doi:10.1002/nme.2025)
21. Sepahvand K, Marburg S. 2014 Stochastic FEM to structural vibration with parametric uncertainty. In *Multiscale modeling and uncertainty quantification of materials and structures* (eds M Papadrakakis and G Stefanou), pp. 299–306. Berlin, Germany: Springer.
22. Didier J, Faverjon B, Sinou JJ. 2012 Analyzing the dynamic response of a rotor system under uncertain parameters by polynomial chaos expansion. *J. Vib. Control* **18**, 712–732. (doi:10.1177/1077546311404269)
23. Blatman G, Sudret B. 2011 Adaptive sparse polynomial chaos expansion based on least angle regression. *J. Comput. Phys.* **230**, 2345–2367. (doi:10.1016/j.jcp.2010.12.021)
24. Nouy A. 2007 A generalized spectral decomposition technique to solve a class of linear stochastic partial differential equations. *Comput. Methods Appl. Mech. Eng.* **196**, 4521–4537. (doi:10.1016/j.cma.2007.05.016)
25. Nouy A. 2008 Generalized spectral decomposition method for solving stochastic finite element equations: invariant subspace problem and dedicated algorithms. *Comput. Methods Appl. Mech. Eng.* **197**, 4718–4736. (doi:10.1016/j.cma.2008.06.012)
26. Nouy A. 2009 Recent developments in spectral stochastic methods for the numerical solution of stochastic partial differential equations. *Arch. Comput. Methods Eng.* **16**, 251–285. (doi:10.1007/s11831-009-9034-5)
27. Audouze C, Nair PB. 2012 Galerkin reduced-order modeling scheme for time-dependent randomly parametrized linear partial differential equations. *Int. J. Numer. Methods Eng.* **92**, 370–398. (doi:10.1002/nme.4341)
28. Sapsis TP, Lermusiaux PF. 2009 Dynamically orthogonal field equations for continuous stochastic dynamical systems. *Physica D* **238**, 2347–2360. (doi:10.1016/j.physd.2009.09.017)
29. Cheng M, Hou TY, Zhang Z. 2013 A dynamically bi-orthogonal method for time-dependent stochastic partial differential equations I: derivation and algorithms. *J. Comput. Phys.* **242**, 843–868. (doi:10.1016/j.jcp.2013.02.033)
30. Chevreuil M, Nouy A. 2012 Model order reduction based on proper generalized decomposition for the propagation of uncertainties in structural dynamics. *Int. J. Numer. Methods Eng.* **89**, 241–268. (doi:10.1002/nme.3249)
31. Hoeffding W. 1948 A class of statistics with asymptotically normal distribution. *Ann. Math. Stat.* **19**, 293–325. (doi:10.1214/aoms/1177730196)
32. Efron B, Stein C. 1981 The jackknife estimate of variance. *Ann. Stat.* **9**, 586–596. (doi:10.1214/aos/1176345462)
33. Rabitz H, Aliş ÖF. 1999 General foundations of high-dimensional model representations. *J. Math. Chem.* **25**, 197–233. (doi:10.1023/A:1019188517934)
34. Griebel M. 2006 Sparse grids and related approximation schemes for higher dimensional problems. In *Foundations of computational mathematics* (*FoCM05*), *santander* (eds LM Pardo, A Pinkus, E Suli, MJ Todd), pp. 106–161. Cambridge, UK: Cambridge University Press.
35. Yang X, Choi M, Lin G, Karniadakis GE. 2012 Adaptive ANOVA decomposition of stochastic incompressible and compressible flows. *J. Comput. Phys.* **231**, 1587–1614. (doi:10.1016/j.jcp.2011.10.028)

36. Foo J, Karniadakis GE. 2010 Multi-element probabilistic collocation method in high dimensions. *J. Comput. Phys.* **229**, 1536–1557. (doi:10.1016/j.jcp.2009.10.043)
37. Ma X, Zabaras N. 2010 An adaptive high-dimensional stochastic model representation technique for the solution of stochastic partial differential equations. *J. Comput. Phys.* **229**, 3884–3915. (doi:10.1016/j.jcp.2010.01.033)
38. Rahman S. 2008 A polynomial dimensional decomposition for stochastic computing. *Int. J. Numer. Methods Eng.* **76**, 2091–2116. (doi:10.1002/nme.2394)
39. Nair PB, Håkansson P. 2010 Prospects for overcoming the curse of dimensionality in polynomial chaos based stochastic projection schemes. In *Proc. of the 4th European Conf. on Computational Mechanics*. Paris, France. See https://www.eccm-2010.org/abstract_pdf/abstract_1952.pdf.
40. Audouze C, Nair PB. 2014 Anchored ANOVA Petrov–Galerkin projection schemes for parabolic stochastic partial differential equations. *Comput. Methods Appl. Mech. Eng.* **276**, 362–395. (doi:10.1016/j.cma.2014.02.023)
41. Friedman JH. 1991 Multivariate adaptive regression splines. *Ann. Stat.* **19**, 1–67. (doi:10.1214/aos/1176347963)
42. Li G, Wang SW, Rabitz H, Wang S, Jaffé P. 2002 Global uncertainty assessments by high dimensional model representations (HDMR). *Chem. Eng. Sci.* **57**, 4445–4460. (doi:10.1016/S0009-2509(02)00417-7)
43. Loève M. 1977 *Probability theory*. Berlin, Germany: Springer.
44. Zhang J, Ellingwood B. 1994 Orthogonal series expansions of random fields in reliability analysis. *J. Eng. Mech.* **120**, 2660–2677. (doi:10.1061/(ASCE)0733-9399(1994)120:12(2660))
45. Schwab C, Todor RA. 2006 Karhunen–Loève approximation of random fields by generalized fast multipole methods. *J. Comput. Phys.* **217**, 100–122. (doi:10.1016/j.jcp.2006.01.048)
46. Bathe KJ. 1996 *Finite element procedures*. Upper Saddle River, NJ: Prentice-Hall.